ACS OMEGA

http://pubs.acs.org/journal/acsodf

Article

Promotion of TiO_2 Nanotube-Confined Pt Nanoparticles via Surface Modification with Fe_2O_3 for Ethylene Oxidation at Low Temperature

Juan Li, Liangpeng Wu, Nan Wang, Xinjun Li,* and Chaoping Cen*

Cite This: *ACS Omega* 2021, 6, 11529−11536

Read Online

ACCESS | Metrics & More | Article Recommendations | Supporting Information

ABSTRACT: A modified confined catalyst with Pt nanoparticles on the interior and Fe_2O_3 on the exterior surface of TiO_2 nanotubes (Pt-in/Fe_2O_3-TNTs) was prepared and investigated for catalyzing the oxidation of ethylene. Compared with the Pt-in/TNTs without Fe_2O_3 modification, the Pt-in/Fe_2O_3-TNTs exhibited a significantly enhanced activity, and the complete conversion temperature of ethylene decreased from 170 to 95 °C. X-ray photoelectron spectroscopy analysis indicated that the Pt nanoparticles were stabilized at higher oxidation states in the Pt-in/Fe_2O_3-TNT catalyst. It was proposed that the modification of Fe_2O_3 on the outer surface can tune the electronic state of the encapsulated Pt particles and accelerate the electrons transferred from Pt to Fe species via TiO_2 nanotubes, thus improving the catalytic oxidation performance of the confined catalyst.

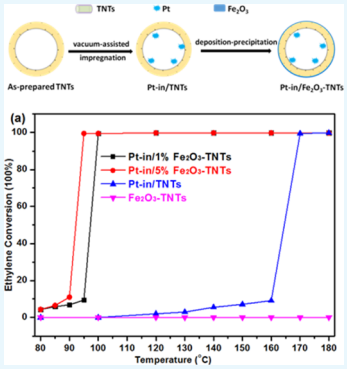

INTRODUCTION

Ethylene, a low-molecular-weight gaseous volatile organic compound (VOC), is widely used as a raw material in chemical industry, which will lead to photochemical pollution of the atmosphere and cause anesthetic illness.[1] Moreover, ethylene released from fruits and vegetables can also accelerate the maturation and decay of produce.[2,3] Therefore, the removal of ethylene contaminant from air under mild conditions is of great necessity. Low-temperature catalytic oxidation is one of the most important and effective methods for transforming ethylene to harmless carbon dioxide and water.

Until now, some solid thermal catalysts have been attempted for the oxidation of ethylene, such as Au/Co_3O_4,[4] Pt/MnO_2,[5] Cu/MnO_2,[6] Ag/ZSM-5,[7,8] Pd/ZSM-5,[9] Pt/ZSM-5,[10] Pt/MCM-41,[11] Pt/SBA-15,[12,13] Pt/C,[14] Pt/YSZ,[15,16] Ru/YSZ,[16] Pt/ZrO_2,[11] Pt/TiO_2,[11] and Pt/SiO_2.[17] Among these catalysts, supported Pt catalysts have attracted wide interest because of their superior activity in catalyzing the oxidation of ethylene at relatively low temperatures. It was reported that the Pt/MCM-41 showed higher activity to catalytically remove C_2H_4 than other noble metals (Pd, Au, or Ag) loaded on the same support.[11] Although the conversion of trace ethylene over Pt nanoparticles supported on zeolites and mesoporous silica reached 100% at 0 °C, the activity of these low-temperature catalysts decreased rapidly and did not meet the requirements for practical applications.[10−13] Pt catalysts with metal oxides (such as Al_2O_3, ZrO_2, TiO_2, YSZ, and MnO_2) as supports were also widely studied for the oxidation of ethylene in view of the synergetic catalytic effect between noble metals and metal oxides.[5,11,15−17] However, most of these catalysts showed relatively low catalytic activities, and the temperature for the complete conversion of ethylene was usually higher than 100 °C. It is therefore still a great challenge to develop a catalytic material with enhanced low-temperature activity and excellent cycle stability toward the complete oxidation of ethylene.

The confinement of the active species inside a nanotube space has been proved as an efficient strategy to improve the catalytic performance. Bao research group[18−20] reported that the confinement within carbon nanotubes (CNTs) can strengthen the electrons transferred from the metal to the carbon surface and hinder the sintering of the encapsulated active component, thereby significantly enhancing the activity and stability of the catalysts. In our previous works, we have successfully entrapped noble metals into titanium dioxide nanotubes (TNTs) and found that TNTs exhibited a similar confinement effect as CNTs due to the unique tubular morphology.[21−23] The performances of phenol hydrogenation, catalytic combustion, and photocatalytic hydrogen production were notably enhanced when Pt, Pd, and Au nanoparticles were entrapped into TNTs.[21−23] It is known that the curvature of nanotube walls causes the electron density to shift from the concave inner to the convex outer surface, which makes the nanotube exist with an electron-deficient interior and electron-enriched exterior surface.[24,25] Regulating the electron proper-

Received: February 4, 2021
Accepted: April 6, 2021
Published: April 20, 2021

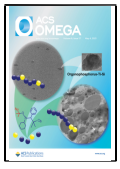

Scheme 1. Synthetic Route for the Pt-in/Fe_2O_3-TNT Catalyst

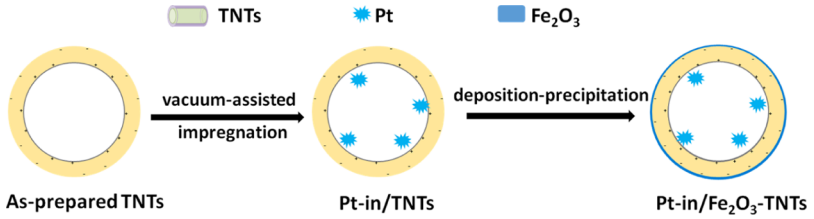

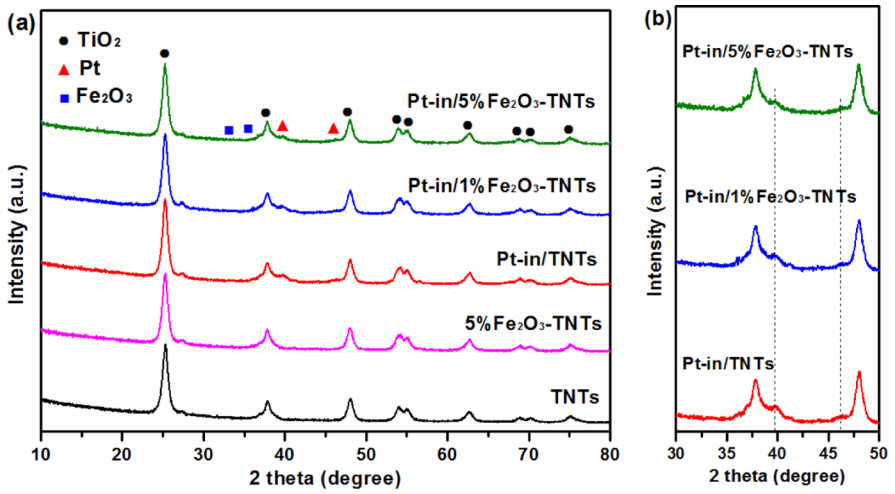

Figure 1. (a) XRD patterns of the as-prepared catalysts and (b) the zooming in the regions of Pt peaks (2θ = 30−50°).

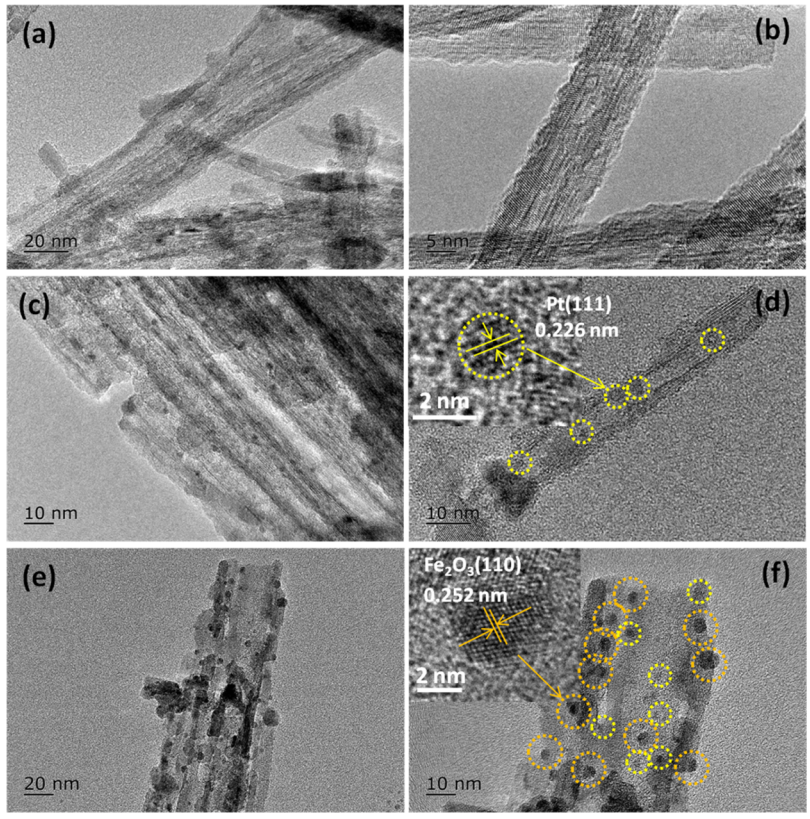

Figure 2. TEM and HRTEM images of the prepared catalysts: (a,b) TNTs, (c,d) Pt-in/TNTs, and (e,f) Pt-in/5% Fe_2O_3-TNTs.

ties of materials by introducing an electron-withdrawing group is another effective method to improve the catalyst performance.[17,26−29] Nanometer iron oxide (Fe_2O_3) was intensively studied in the fields of thermal-, electro-, and photocatalysis.[30−32] As a variable valence metal oxide with the property of binding electrons, Fe_2O_3 can easily capture

https://doi.org/10.1021/acsomega.1c00665
ACS Omega 2021, 6, 11529−11536

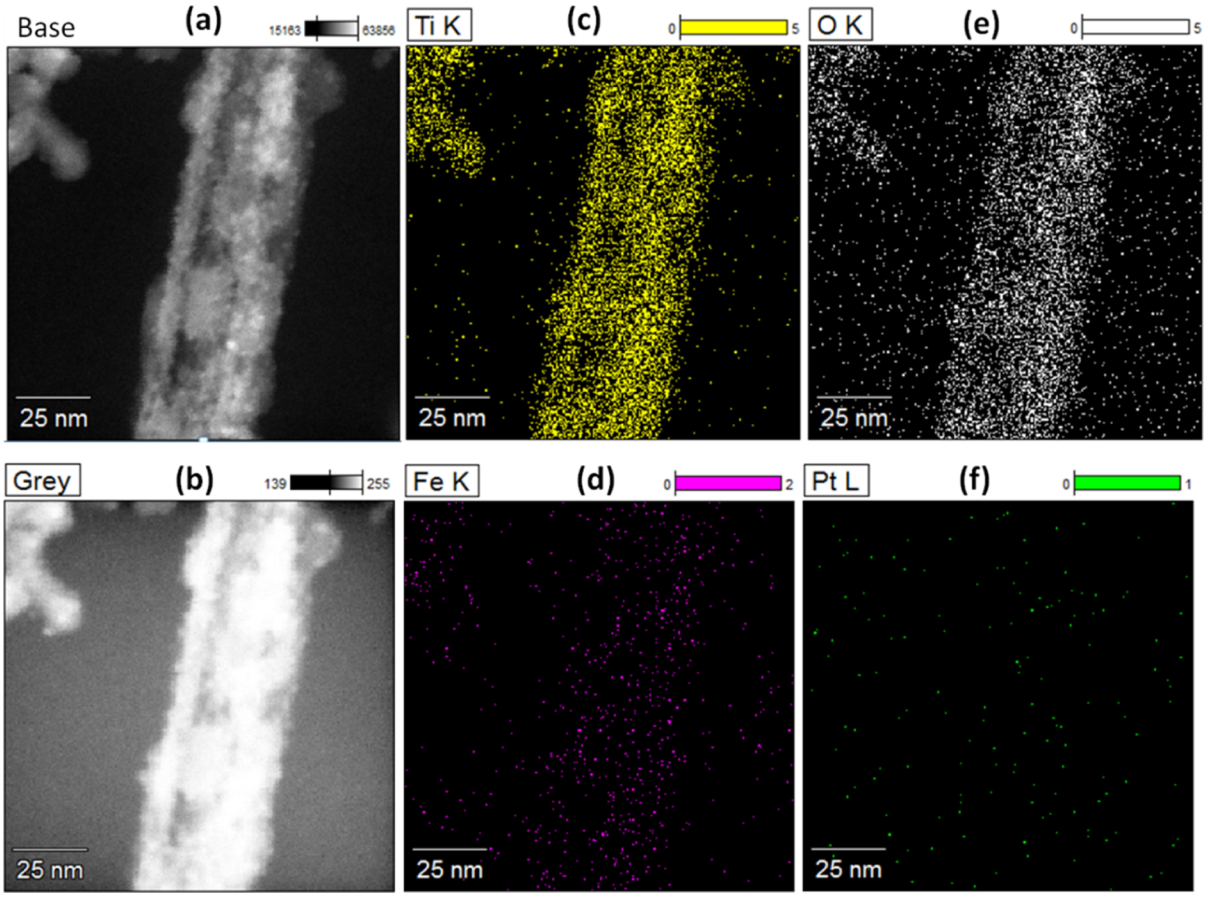

Figure 3. HAADF-STEM images and STEM−EDX elemental mappings of the Pt-in/5% Fe_2O_3-TNTs: (a) base, (b) gray, (c) Ti, (d) Fe, (e) O, and (f) Pt.

electrons and get reduced into Fe_3O_4. Therefore, the electron property of the encapsulated active component can be further regulated by coupling Fe_2O_3 on the outside wall of TNTs. Our previous study has revealed that the electronic state of Pd is significantly enhanced when it is modified with Fe_2O_3 nanoparticles.[29] As a result, the modified catalysts presented a significantly improved activity for the photocatalytic degradation of methyl orange. The confined Pt nanoparticles are considered highly active and promising catalysts for the combustion of VOCs. The modulation on the electronic property of the Pt catalysts will provide some insights for the design of highly efficient catalytic combustion catalysts.

In the present work, a modified confined catalyst, with Pt nanoparticles inside and Fe_2O_3 on the outside surface of TNTs (Pt-in/Fe_2O_3-TNTs), was successfully fabricated using vacuum-assisted incipient-wetness impregnation and deposition−precipitation methods (Scheme 1). The ethylene oxidation performance of Pt-in/Fe_2O_3-TNTs was compared with that of the confined Pt catalyst (Pt-in/TNTs) without Fe_2O_3 modification. The contribution of Fe_2O_3 modification toward the modulation of electron structure and the enhancement of catalytic oxidation activity was discussed in detail.

RESULTS AND DISCUSSION

Figure 1 shows the XRD patterns of the TNTs, Fe_2O_3-TNTs, Pt-in/TNTs, and Pt-in/Fe_2O_3-TNTs samples. All samples display the characteristic peaks of anatase TiO_2 (JCPDS no. 21-1272). The relative weak peaks at 2θ = 39.8 and 46.2° can be differentiated in the Pt-in/TNTs and Pt-in/Fe_2O_3-TNTs catalysts, corresponding to the (111) and (002) planes of the metallic Pt crystalline phase (JCPDS no. 04-0802). It is observed from zooming in of the regions of 2θ = 30−50° that the diffraction peaks of metallic Pt are slightly weakened with the deposition of iron oxide on the catalyst surface. These results imply that an interaction between Pt particles and iron oxide may be present in the Pt-in/Fe_2O_3-TNT catalysts. No distinct diffraction peaks indexed to the Fe_2O_3 phase are observed in the XRD patterns of the Fe_2O_3-TNTs and Pt-in/Fe_2O_3-TNTs samples, which might be due to the hindrance by the strong TiO_2 peaks or the formation of amorphous particles which are below the XRD detection limit. For comparison, pure Fe_2O_3 was obtained by the precipitation method using $Fe(NO_3)_3{\cdot}9H_2O$ as the iron resource and Na_2CO_3 as the precipitation agent. For the pure Fe_2O_3 calcined at 250 °C under an air atmosphere, the weak diffraction peaks appear at 2θ = 24.1, 33.1, 35.6, 40.8, 49.4, and 54.0° (see Figure S1), which could be associated with the presence of the α-Fe_2O_3 phase.

Figure 2 shows the TEM and high-resolution TEM (HRTEM) images of pristine TNTs, Pt-in/TNTs, and Pt-in/5% Fe_2O_3-TNTs samples. It can be seen from Figure 2a−b that the pristine TNTs display one-dimensional nanotubular morphology with a relative smooth and clean outside surface. Also, the TNTs obtained are multilayered nanotubes with the outer diameter of 9−12 nm and the inner one of 5−8 nm. For the Pt-in/TNTs and the Pt-in/5%Fe_2O_3-TNTs, most of the Pt nanoparticles with the average size of 2−3 nm are successfully confined within the inner cavity of the TiO_2 nanotube, as

https://doi.org/10.1021/acsomega.1c00665
ACS Omega 2021, 6, 11529−11536

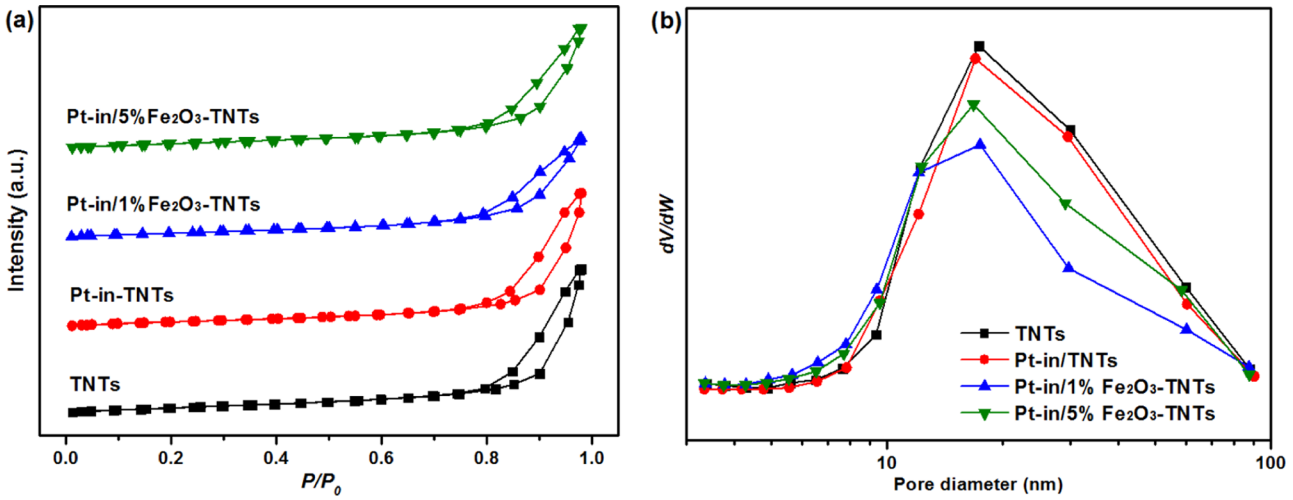

Figure 4. (a) N_2 adsorption−desorption isotherms and (b) pore size distributions of the samples.

Table 1. Textural and Chemical Properties of the As-Prepared Samples

sample	S_{BET} (m^2/g)	V_p[a] (cm^3/g)	D_p[a] (nm)	D_{Pt}[b] (nm)	Pt[c] (wt %)	Fe_2O_3[c] (wt %)	atomic ratio[c] Pt/Ti/Fe
TNTs	151.4	0.79	17.3				
Pt-in/TNTs	120.4	0.74	16.9	2−3	2.01		0.0082/1
Pt-in/1% Fe_2O_3-TNTs	122.4	0.55	12.1	2−3	2.01	1.02	0.0082/1/0.0102
Pt-in/5% Fe_2O_3-TNTs	132.1	0.67	12.3	2−3	2.01	3.46	0.0082/1/0.0346

[a]Porosity data were derived by the Barrett−Joyner−Halenda desorption branch. [b]Average particle sizes were calculated from 200 individual crystallites in TEM images. [c]The actual loading contents of Pt and Fe_2O_3 and the atomic ratio of Pt/Ti/Fe were determined by ICP-AES.

shown in Figure 2c−f. The HRTEM image (the inset of Figure 2d) recorded from the region marked with yellow circles shows a lattice spacing of 0.226 nm, which corresponds to the metal Pt (111) plane. The filling of Pt nanoparticles inside the nanotube can be attributed to the capillary effect derived from the vacuum-assisted impregnation procedure.[21−23] For the Pt-in/5% Fe_2O_3-TNTs, Fe_2O_3 particles are well dispersed on the external surface of TNTs, as depicted by the orange circles with a measured lattice spacing of 0.252 nm corresponding to the Fe_2O_3 (110) plane (Figure 2e−f). The particle size distributions of Pt from the TEM analysis are provided in the Supporting Information (see Figure S2).

High-angle annular dark field (HAADF)-STEM images and STEM−EDX elemental mappings of the Pt-in/Fe_2O_3-TNTs were performed to further determine the distribution of elements. As shown in Figure 3, better distribution and coexistence of Ti, O, Pt, and Fe elements can be found for the Pt-in/Fe_2O_3-TNTs, implying that Pt and Fe_2O_3 nanoparticles are dispersed uniformly in/on the TNTs. STEM−EDX spectrum and quantitative results of the Pt, Fe, and Ti elements for the Pt-in/5% Fe_2O_3-TNT catalyst are provided in the Supporting Information (see Figure S3). The Pt/Ti/Fe atomic ratio is calculated to be 0.0059/1/0.0528. Compared with the value determined by inductively coupled plasma atomic emission spectroscopy (ICP-AES) (Pt/Ti/Fe atomic ratio = 0.0082/1/0.0346), the Fe signal is enhanced at the TiO_2 edge, further confirming that Fe_2O_3 is deposited on the outer surface of the nanotubes.

Figure 4 shows the N_2 adsorption−desorption isotherms and pore size distribution curves of the synthesized samples. The corresponding surface area (S_{BET}), pore volume (V_p), and average pore size (D_p) are summarized in Table 1. All samples exhibit typically a BDDT Type III isotherm with a large type H3 hysteresis hoop according to the Brunauer−Deming−Deming−Teller classification. The support of TNTs has a surface area of 151.4 m^2/g and a pore volume of 0.79 cm^3/g. The surface area, pore volume, and pore size decrease on loading Pt on TNTs. For the Pt-in/TNTs and Pt-in/Fe_2O_3-TNTs samples, the surface area and pore volume are clearly lower than those of the TNTs. This can be explained by the fact that Pt nanoparticles are confined within the inner cavity of TiO_2 nanotubes via the vacuum-assisted impregnation process and take up some of the pore volume. The actual loading contents of Pt and Fe_2O_3 in the samples were determined by ICP-AES, as shown in Table 1. The actual loading of Pt is 2.01 wt % for the as-prepared catalysts, and the actual loading of Fe_2O_3 is 1.06 wt % for the Pt-in/1% Fe_2O_3-TNTs and 3.46 wt % for the Pt-in/5% Fe_2O_3-TNTs, respectively.

X-ray photoelectron spectroscopy (XPS) measurements were conducted to investigate the chemical states of the surface elements in the samples. The photoelectron peaks corresponding to Fe 2p, O 1s, Ti 2p, C 1s, and Pt 4f can be detected in the full-survey-scan spectrum for the Fe_2O_3-loaded catalysts (see Figure S4), indicating that the Fe element has been successfully introduced in the synthesized samples. The high-resolution XPS spectra recorded are shown in Figure 5. For the Pt-in/1% Fe_2O_3-TNTs and Pt-in/5% Fe_2O_3-TNTs catalysts, the Fe $2p_{3/2}$ and Fe $2p_{1/2}$ peaks centered at 711.2 and 724.6 eV along with two shakeup satellite peaks at about 719.5 and 732.2 eV are in good agreement with the reported Fe_2O_3 phase (Figure 5a).[34,35] No obvious peaks from Fe^0 and/or Fe^{2+} were observed, indicating that Fe_2O_3 is the only iron species formed on the surface of the Pt-in/Fe_2O_3-TNTs. The Pt 4f XPS spectra can be deconvoluted into two peaks, with the lower binding energy peak corresponding to the Pt $4f_{7/2}$ level

https://doi.org/10.1021/acsomega.1c00665
ACS Omega 2021, 6, 11529−11536

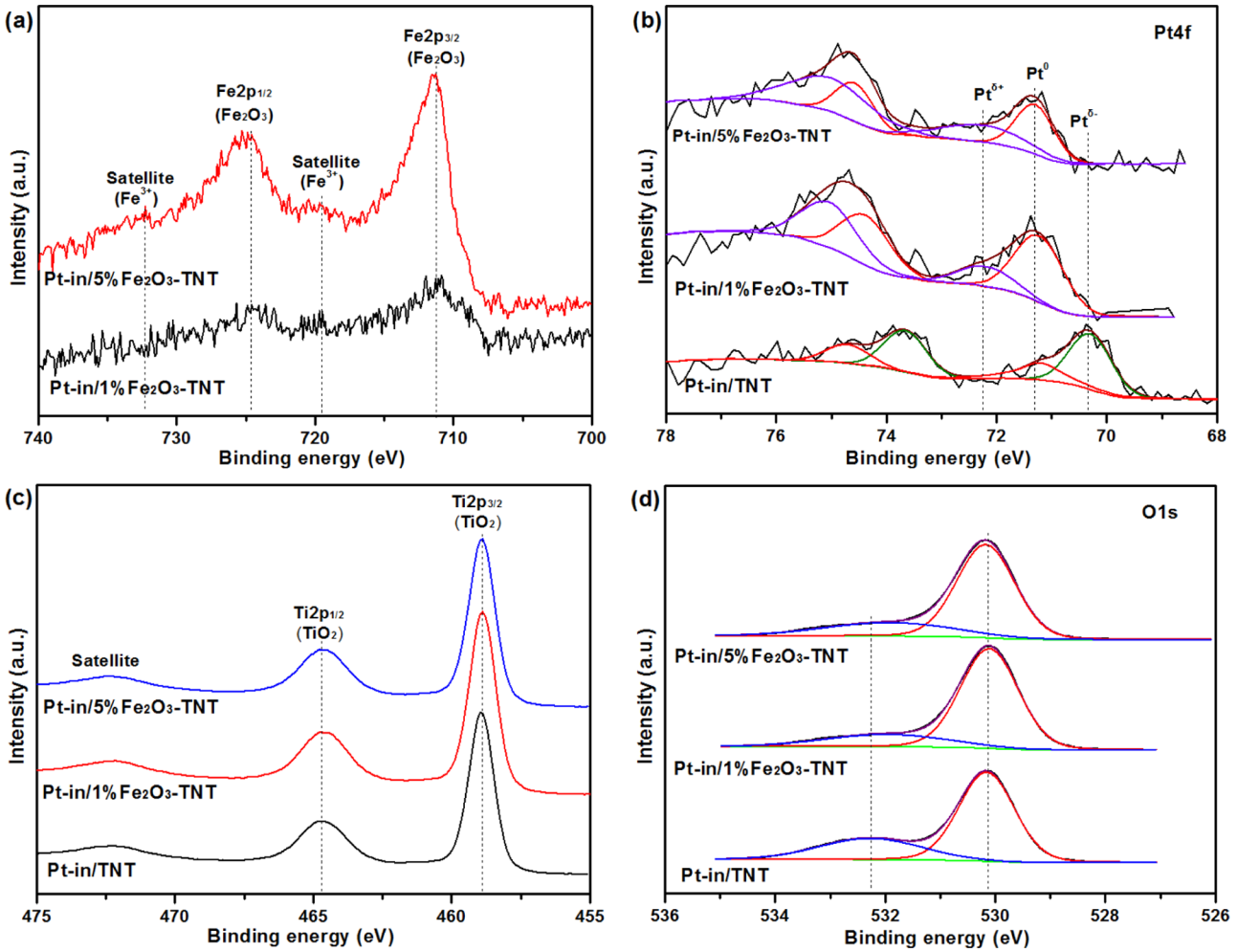

Figure 5. XPS spectra of the prepared catalysts: (a) Fe 2p, (b) Pt 4f, (c) Ti 2p, and (d) O 1s.

Table 2. XPS Results of the As-prepared Catalysts: Binding Energy and Element Percentage

	BE for Pt $4f_{7/2}$ (eV)			element percent (%)			atomic ratio
catalyst	$Pt^{\delta-}$	Pt^0	$Pt^{\delta+}$	$Pt^{\delta-}$	Pt^0	$Pt^{\delta+}$	Pt/Ti/Fe
Pt-in/TNTs	70.3	71.2		68.4	31.6		0.0075/1
Pt-in/1% Fe_2O_3-TNTs		71.2	72.2		74.4	25.6	0.0052/1/0.0316
Pt-in/5% Fe_2O_3-TNTs		71.3	72.3		57.3	42.7	0.0054/1/0.1631

and the higher binding energy peak corresponding to the Pt $4f_{5/2}$ level. For the Pt-in/TNTs, there are two Pt $4f_{7/2}$ peaks centered at 70.3 and 71.2 eV, which can be assigned to $Pt^{\delta-}$ and Pt^0 species, respectively.[28] Modification by Fe_2O_3 significantly changes the profiles of Pt 4f core electrons. Compared with the unmodified Pt-in/TNTs, the Pt $4f_{7/2}$ peaks for the Fe_2O_3-loaded catalysts shift to a higher binding energy value centered at about 71.3 and 72.3 eV (Figure 5b), corresponding to metallic Pt^0 and ionic $Pt^{\delta+}$ species.[10] This implies that the charge is transferred from Pt to Fe_2O_3 species via TiO_2 nanotubes, and Pt nanoparticles are stabilized at higher oxidation states in the Pt-in/Fe_2O_3-TNTs, indicating the formation of strong metal−support interactions between Pt and TNTs. As a result, the electron density of the Pt nanoparticles is affected by the modification of Fe_2O_3 nanoparticles on the outside wall of the TNTs. Moreover, the modification of Fe_2O_3 on the TNTs does not change the XPS spectra of Ti 2p. As shown in Figure 5c, the Ti $2p_{3/2}$ and Ti $2p_{1/2}$ centered at 458.9 and 464.7 eV are assigned to Ti^{4+} for all samples. The integral peak of O 1s can be divided into two peaks concentrated at approximately 530.1 and 532.2 eV (Figure 5d), corresponding to oxygen in the composition of titanium oxide and oxygen in the composition of OH group or water. The surface atomic ratios of the different Pt species ($Pt^{\delta+}/Pt^0/Pt^{\delta-}$) and the Pt/Ti/Fe for all samples are listed in Table 2. The $Pt^{\delta+}/(Pt^0 + Pt^{\delta+})$ ratios in the Pt-in/Fe_2O_3-TNT samples are significantly increased with the deposition of Fe_2O_3 on the outer surface of TNTs (25.6% for Pt-in/1% Fe_2O_3-TNTs vs 42.7% for Pt-in/5% Fe_2O_3-TNTs). As is known, the inner surface of TNTs is in an electron-deficient state, and such a state is further strengthened by introducing an electron-withdrawing group (Fe_2O_3) on the outer surface. Meantime, the position of the conduction band of Fe_2O_3 (0.28 eV) is lower than that of anatase TiO_2 (−0.29 eV) in terms of energy level of the materials. The difference in conduction band positions will drive the electron to transfer from TNTs to

https://doi.org/10.1021/acsomega.1c00665
ACS Omega 2021, 6, 11529−11536

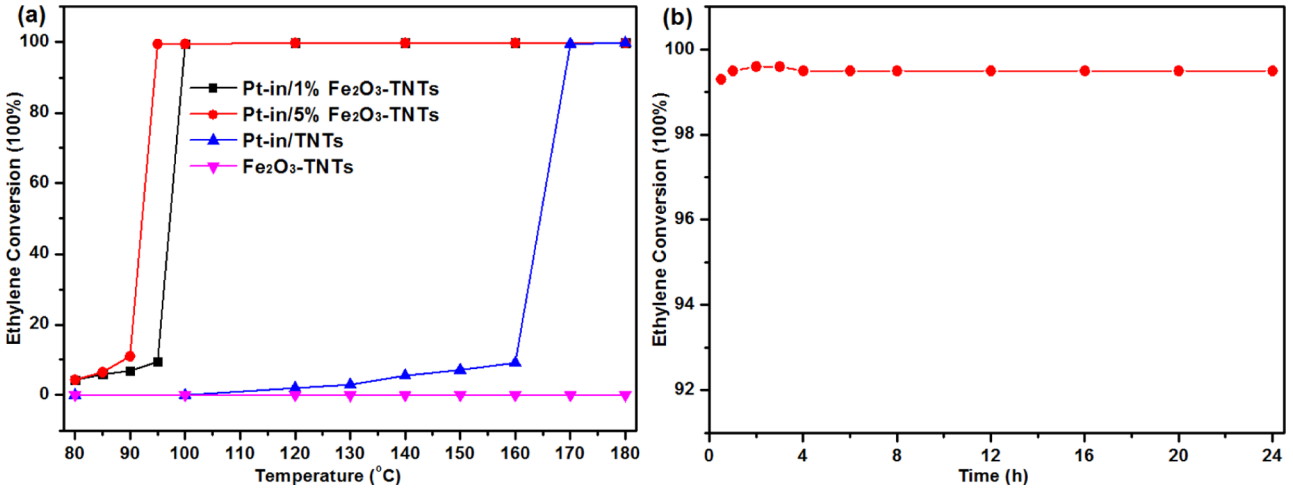

Figure 6. (a) Conversion curves for ethylene oxidation over the different catalysts and (b) reaction tests at 95 °C for ethylene oxidation with time-on-stream over Pt-in/5% Fe_2O_3-TNTs. Reaction conditions: C_2H_4 = 2.0 vol %, O_2 = 49.0 vol %, Ar balance, GHSV = 24,000 mL/(g h).

Fe_2O_3 particles crossing the interface. Therefore, the encapsulated Pt species are stabilized at higher oxidation states in the Pt-in/Fe_2O_3-TNT samples, which would exert further influence on their oxidation activity. Furthermore, it also can be seen from the results of XPS and ICP-AES that the Fe/Ti atomic ratios on the surface for the Pt-in/Fe_2O_3-TNT catalysts are much larger than that in the bulk (see Tables 1 and 2), indicating that Fe_2O_3 is highly dispersed on the outer surface of TNTs.

The catalytic performances of Fe_2O_3-TNTs, Pt-in/TNTs, and Pt-in/Fe_2O_3-TNTs catalysts for ethylene oxidation were investigated under the flow of 2.0% C_2H_4/49% O_2/Ar. Figure 6 shows the curves of ethylene conversion over the different catalysts. The conversion of ethylene over the Fe_2O_3-TNTs is extremely low, suggesting that the oxidation of ethylene cannot proceed at all in the absence of Pt nanoparticles below 200 °C. The Pt-in/TNTs exhibit complete conversion of C_2H_4 to CO_2 at 170 °C. After the modification by Fe_2O_3, the ethylene oxidation activities of the catalysts are obviously improved. The complete conversion temperature of ethylene decreases from 170 to 100 °C and 95 °C for the Pt-in/1% Fe_2O_3-TNTs and Pt-in/5% Fe_2O_3-TNTs, respectively. In comparison with the Pt-in/1% Fe_2O_3-TNTs, the Pt-in/5% Fe_2O_3-TNTs show a slightly lower temperature for complete oxidation of ethylene. Furthermore, the Pt-in/5% Fe_2O_3-TNTs demonstrate pretty good long-term stability, with no decay of catalytic activity over 24 h successive ethylene oxidation test at 95 °C, as shown in Figure 5b.

Our previous studies have found that the confinement within TNTs can tune the electronic states of the encapsulated active component and strengthen the electrons transferred from the metal (Pt, Pd, or Au) to the nanotube surface.[21−23] In the meantime, the electronic properties of the encapsulated active component can be further regulated when an electron-withdrawing group is introduced, thus resulting in an enhanced catalytic activity.[28,29] In the present work, Fe_2O_3 was used to further regulate the electron density distribution of the confined Pt catalyst. Due to Fe_2O_3 with the property of binding electrons ($Fe^{3+} + e \rightarrow Fe^{2+}$), electrons are transferred from the interior to the exterior surface of TNTs. As a result, the entrapped Pt particles are stabilized at higher oxidation states and thus possess a great quantity of active oxygen species, which would make it much easier to adsorb reactant molecules and reduce their free energy, favoring the C_2H_4 oxidation reaction. On the contrary, after partial reduction of Fe_2O_3 to Fe_3O_4, the obtained Pt-in/5% Fe_3O_4-TNT catalyst exhibits the worse ethylene oxidation performance (see Figure S5). In order to characterize the presence of Fe_3O_4, the reduced FeO_x was obtained by a further reduction of pure Fe_2O_3 at 250 °C for 4 h under 8% H_2−Ar atmosphere, and the corresponding XRD patterns were recorded. After the pure Fe_2O_3 was annealed under 8% H_2−Ar atmosphere, the crystal phase structure of Fe_3O_4 (JCPDS no. 65-3107) can be identified in the XRD patterns, as shown in Figure S6. This further proves that heat treatment under 8% H_2−Ar atmosphere at 250 °C for 4 h can partially reduce Fe_2O_3 to Fe_3O_4. It is inferred that Fe_3O_4 is an electron-donating component, which would suppress the electron migration from the inside to the outside surface of TNTs and hence exhibit a reduced oxidation activity. A higher percentage for ionic $Pt^{\delta+}$ species in the modified confined catalyst has been verified from the XPS analysis (see Figure 5 and Table 2). The Pt particles with higher oxidation states are believed to be promising for catalytic combustion.[10,28] As one-dimensional nanomaterials, TiO_2 nanotubes have good electron transport characteristics. Owing to the unique structure of the catalyst with Pt nanoparticles inside and Fe_2O_3 on the outside surface of TNTs, the transformation of $Fe^{3+} \rightarrow Fe^{2+}$ could accelerate the electron transferred from Pt to Fe species via TiO_2 nanotubes, facilitating the formation and migration of active oxygen species in the catalyst. Therefore, the catalytic activity for ethylene oxidation over the Pt-in/Fe_2O_3-TNTs is significantly improved by Fe_2O_3 modification.

CONCLUSIONS

In summary, Fe_2O_3-decorated TiO_2 nanotube-confined Pt nanoparticles (Pt-in/Fe_2O_3-TNTs) was successfully synthesized by vacuum-assisted impregnation and deposition−precipitation methods. The Pt-in/Fe_2O_3-TNTs exhibit a significantly enhanced catalytic performance and a lower temperature for complete oxidation of ethylene than the Pt-in/TNTs. The improved catalytic oxidation performance can be ascribed to the modulation of electronic states for the encapsulated Pt particles by Fe_2O_3 modification on the exterior surface of TNTs. This study provides a prospect for VOC

https://doi.org/10.1021/acsomega.1c00665
ACS Omega 2021, 6, 11529−11536

purification by Fe_2O_3-modified TiO_2 nanotube-confined catalysts toward low-temperature applications.

EXPERIMENTAL SECTION

Catalyst Preparation. TNTs were synthesized via a hydrothermal method according to our previous report.[33] In a typical procedure, NaOH solution (10 M, 360 mL) and P25 powder (6 g) were added to a 500 mL Teflon-lined flask and refluxed at 110 °C under atmospheric pressure, keeping magnetic stirring for 48 h. The hydrothermally treated powders were collected and washed thoroughly with deionized water. The obtained precipitate was immersed into HCL solution (0.1 M) for 5 h and rinsed with deionized water until pH ∼ 7. The product was dried at 60 °C overnight and calcined at 350 °C for 2 h.

The Pt-in/TNT catalyst was prepared via a vacuum assisted incipient-wetness impregnation method. Briefly, 5.4 mL of $H_2PtCl_6{\cdot}6H_2O$ ethanol solution (1.0 g/100 mL) was added dropwise into a round-bottom flask containing 1.0 g TNT powder to achieve nominal Pt loading of 2 wt %. The resulting slurry was vacuumed at room temperature until the excess solvent was evaporated completely. Finally, the dried powder was reduced at 250 °C for 4 h under 8% H_2−Ar atmosphere.

The Pt-in/Fe_2O_3-TNT catalyst was prepared by a deposition−precipitation method. Typically, 0.5 g of Pt-in/TNT powders were dispersed in 40 mL of aqueous solution containing a calculated amount of $Fe(NO_3)_3{\cdot}9H_2O$. The pH was adjusted to ∼8 with 0.1 M Na_2CO_3 aqueous solution. The mixture was then aged at 60 °C for 3 h under stirring. After filtration and being washed with deionized water, the powder was dried at 60 °C and subsequently calcined at 250 °C for 4 h under air atmosphere. The nominal loading of Fe_2O_3 on TNTs was 1 and 5 wt % and labeled as Pt-in/1% Fe_2O_3-TNTs and Pt-in/5% Fe_2O_3-TNTs, respectively.

Catalyst Characterization. Surface area and porosity of the samples were analyzed by N_2 adsorption−desorption using a SI-MP-10 automated system at liquid nitrogen temperature after the samples were degassed in a vacuum at 180 °C for 5 h. Powder XRD patterns were recorded using a PANalytical X'Pert Pro diffractometer with a Cu Kα radiation source operated at 40 kV and 40 mA. The morphologies of the samples were observed by HRTEM (FEI Tecnai G20). XPS was performed by a Thermo Fisher Scientific ESCALAB 250XI spectrometer with a monochromatized Al Kα source (1486.6 eV). The C 1s line was taken as an internal standard at 284.8 eV. The actual loading contents of Pt and Fe_2O_3 in the samples were determined by ICP-AES on a Plasma-Spec-I spectrometer.

Catalytic Activity Test. The catalytic oxidation performance for ethylene was tested in a continuous flow fixed-bed quartz reactor under atmospheric pressure. 100 mg samples were placed between two layers of quartz wool inside a quartz tube (i.d. = 6 mm) and heated at a rate of 1 °C/min and kept for 0.5 h under target temperature. The typical feed gas composition was 2% ethylene/49% O_2 balanced with Ar with a total flow rate of 40 mL/min. Effluents (ethylene, CO, and CO_2) from the reactor were analyzed by an Agilent 7890A gas chromatograph equipped with thermal conductivity and flame ionization detectors.

ASSOCIATED CONTENT

Supporting Information

The Supporting Information is available free of charge at https://pubs.acs.org/doi/10.1021/acsomega.1c00665.

XRD patterns of pristine Fe_2O_3, Pt Particle size distributions, STEM−EDX spectrum, XPS survey spectra, conversion curve for ethylene oxidation over the Pt-in/5% Fe_3O_4-TNTs, and XRD patterns of reduced FeO_x (PDF)

AUTHOR INFORMATION

Corresponding Authors

Xinjun Li − *Key Laboratory of Renewable Energy, Guangzhou Institute of Energy Conversion, Chinese Academy of Sciences, Guangzhou 510640, China;* orcid.org/0000-0003-0220-9003; Email: lixj@ms.giec.ac.cn

Chaoping Cen − *South China Institute of Environmental Science, Ministry of Environmental Protection, Guangzhou 510655, China;* orcid.org/0000-0001-6176-8476; Email: cenchaoping@scies.org

Authors

Juan Li − *Key Laboratory of Renewable Energy, Guangzhou Institute of Energy Conversion, Chinese Academy of Sciences, Guangzhou 510640, China*

Liangpeng Wu − *Key Laboratory of Renewable Energy, Guangzhou Institute of Energy Conversion, Chinese Academy of Sciences, Guangzhou 510640, China*

Nan Wang − *Key Laboratory of Renewable Energy, Guangzhou Institute of Energy Conversion, Chinese Academy of Sciences, Guangzhou 510640, China*

Complete contact information is available at: https://pubs.acs.org/10.1021/acsomega.1c00665

Notes

The authors declare no competing financial interest.

ACKNOWLEDGMENTS

This study was funded by the Natural Science Foundation of Guangdong Province (no. 2018A0303130212), the Science and Technology Project of Guangzhou, China (no. 201803030019), and the Foundation of Guangdong Province Engineering Laboratory for Air Pollution Control (no. 2019323609-01). The authors thank the support from the Analytical & Testing Center, Guangzhou Institute of Energy Conversion, Chinese Academy of Sciences, China.

REFERENCES

(1) Trinh, Q. H.; Lee, S. B.; Mok, Y. S. Removal of Ethylene from Air Stream by Adsorption and Plasma-Catalytic Oxidation Using Silver-Based Bimetallic Catalysts Supported on Zeolite. *J. Hazard. Mater.* **2015**, *285*, 525−534.

(2) Keller, N.; Ducamp, M.-N.; Robert, D.; Keller, V. Ethylene Removal and Fresh Product Storage: A Challenge at the Frontiers of Chemistry. Toward an Approach by Photocatalytic Oxidation. *Chem. Rev.* **2013**, *113*, 5029−5070.

(3) Pan, X.; Chen, X.; Yi, Z. Defective, Porous TiO_2 Nanosheets with Pt Decoration as an Efficient Photocatalyst for Ethylene Oxidation Synthesized by a C_3N_4 Templating Method. *ACS Appl. Mater. Interfaces* **2016**, *8*, 10104−10108.

(4) Ma, C. Y.; Mu, Z.; Li, J. J.; Jin, Y. G.; Cheng, J.; Lu, G. Q.; Hao, Z. P.; Qiao, S. Z. Mesoporous Co_3O_4 and Au/Co_3O_4 Catalysts for

Low-Temperature Oxidation of Trace Ethylene. *J. Am. Chem. Soc.* **2010**, *132*, 2608−2613.
(5) Wang, M.; Zhang, L.; Huang, W.; Zhou, Y.; Zhao, H.; Lv, J.; Tian, J.; Kan, X.; Shi, J. Pt/MnO_2 Nanosheets: Facile Synthesis and Highly Efficient Catalyst for Ethylene Oxidation at Low Temperature. *RSC Adv.* **2017**, *7*, 14809−14815.
(6) Njagi, E. C.; Genuino, H. C.; King'ondu, C. K.; Dharmarathna, S.; Suib, S. L. Catalytic Oxidation of Ethylene at Low Temperatures Using Porous Copper Manganese Oxides. *Appl. Catal., A* **2012**, *421*−*422*, 154−160.
(7) Yang, H.; Ma, C.; Li, Y.; Wang, J.; Zhang, X.; Wang, G.; Qiao, N.; Sun, Y.; Cheng, J.; Hao, Z. Synthesis, Characterization and Evaluations of the Ag/ZSM-5 for Ethylene Oxidation at Room Temperature: Investigating the Effect of Water and Deactivation. *Chem. Eng. J.* **2018**, *347*, 808−818.
(8) Yang, H.; Ma, C.; Zhang, X.; Li, Y.; Cheng, J.; Hao, Z. Understanding the Active Sites of Ag/Zeolites and Deactivation Mechanism of Ethylene Catalytic Oxidation at Room Temperature. *ACS Catal.* **2018**, *8*, 1248−1258.
(9) Saud, S.; Nguyen, D. B.; Kim, S.-G.; Lee, H. W.; Kim, S. B.; Mok, Y. S. Improvement of Ethylene Removal Performance by Adsorption/Oxidation in a Pin-Type Corona Discharge Coupled with Pd/ZSM-5 Catalyst. *Catalysts* **2020**, *10*, 133.
(10) Yang, H.; Ma, C.; Wang, G.; Sun, Y.; Cheng, J.; Zhang, Z.; Zhang, X.; Hao, Z. Fluorine-enhanced Pt/ZSM-5 catalysts for low-temperature oxidation of ethylene. *Catal. Sci. Technol.* **2018**, *8*, 1988−1996.
(11) Jiang, C.; Hara, K.; Fukuoka, A. Low-Temperature Oxidation of Ethylene over Platinum Nanoparticles Supported on Mesoporous Silica. *Angew. Chem., Int. Ed.* **2013**, *52*, 6265−6268.
(12) Kou, Y.; Sun, L.-B. Size Regulation of Platinum Nanoparticles by Using Confined Spaces for the Low-Temperature Oxidation of Ethylene. *Inorg. Chem.* **2018**, *57*, 1645−1650.
(13) Satter, S. S.; Yokoya, T.; Hirayama, J.; Nakajima, K.; Fukuoka, A. Oxidation of Trace Ethylene at 0 °C over Platinum Nanoparticles Supported on Silica. *ACS Sustainable Chem. Eng.* **2018**, *6*, 11480−11486.
(14) Isaifan, R. J.; Ntais, S.; Baranova, E. A. Particle Size Effect on Catalytic Activity of Carbon-Supported Pt Nanoparticles for Complete Ethylene Oxidation. *Appl. Catal., A* **2013**, *464*−*465*, 87−94.
(15) Isaifan, R. J.; Ntais, S.; Couillard, M.; Baranova, E. A. Size-Dependent Activity of Pt/Yttria-Stabilized Zirconia Catalyst for Ethylene and Carbon Monoxide Oxidation in Oxygen-Free Gas Environment. *J. Catal.* **2015**, *324*, 32−40.
(16) Isaifan, R. J.; Baranova, E. A. Effect of Ionically Conductive Supports on the Catalytic Activity of Platinum and Ruthenium Nanoparticles for Ethylene Complete Oxidation. *Catal. Today* **2015**, *241*, 107−113.
(17) Rioux, R. M.; Hoefelmeyer, J. D.; Grass, M.; Song, H.; Niesz, K.; Yang, P.; Somorjai, G. A. Adsorption and Co-Adsorption of Ethylene and Carbon Monoxide on Silica-Supported Monodisperse Pt Nanoparticles: Volumetric Adsorption and Infrared Spectroscopy Studies. *Langmuir* **2008**, *24*, 198−207.
(18) Chen, W.; Fan, Z.; Pan, X.; Bao, X. Effect of Confinement in Carbon Nanotubes on the Activity of Fischer−Tropsch Iron Catalyst. *J. Am. Chem. Soc.* **2008**, *130*, 9414−9419.
(19) Deng, J.; Yu, L.; Deng, D.; Chen, X.; Yang, F.; Bao, X. Highly Active Reduction of Oxygen on a FeCo Alloy Catalyst Encapsulated in Pod-Like Carbon Nanotubes with Fewer Walls. *J. Mater. Chem. A* **2013**, *1*, 14868−14873.
(20) Zheng, X.; Deng, J.; Wang, N.; Deng, D.; Zhang, W.-H.; Bao, X.; Li, C. Podlike N-Doped Carbon Nanotubes Encapsulating FeNi Alloy Nanoparticles: High-Performance Counter Electrode Materials for Dye-Sensitized Solar Cells. *Angew. Chem., Int. Ed.* **2014**, *53*, 7023−7027.
(21) Yang, X.; Yu, X.; Long, L.; Wang, T.; Ma, L.; Wu, L.; Bai, Y.; Li, X.; Liao, S. Pt Nanoparticles Entrapped in Titanate Nanotubes (TNT) for Phenol Hydrogenation: the Confinement Effect of TNT. *Chem. Commun.* **2014**, *50*, 2794−2796.
(22) Yang, X.; Lu, X.; Wu, L.; Zhang, J.; Huang, Y.; Li, X. Pd Nanoparticles Entrapped in TiO_2 Nanotubes for Complete Butane Catalytic Combustion at 130 °C. *Environ. Chem. Lett.* **2017**, *15*, 421−426.
(23) Han, B.; Wu, L.; Li, J.; Wang, X.; Peng, Q.; Wang, N.; Li, X. A Nanoreactor Based on $SrTiO_3$ Coupled TiO_2 Nanotubes Confined Au Nanoparticles for Photocatalytic Hydrogen Evolution. *Int. J. Hydrogen Energy* **2020**, *45*, 1559−1568.
(24) Pan, X.; Bao, X. The Effects of Confinement Inside Carbon Nanotubes on Catalysis. *Acc. Chem. Res.* **2011**, *44*, 553.
(25) Yu, L.; Li, W.-X.; Pan, X.; Bao, X. In- and Out-Dependent Interactions of Iron with Carbon Nanotubes. *J. Phys. Chem. C* **2012**, *116*, 16461−16466.
(26) Wu, B.; Zheng, N. Surface and Interface Control of Noble Metal Nanocrystals for Catalytic and Electrocatalytic Applications. *Nano Today* **2013**, *8*, 168−197.
(27) Daghrir, R.; Drogui, P.; Robert, D. Photoelectrocatalytic Technologies for Environmental Applications. *J. Photochem. Photobiol., A* **2012**, *238*, 41−52.
(28) Wang, X.; Yang, X.; Miao, L.; Gao, J.; Peng, Q.; Wu, L.; Chen, S.; Li, X. Bi_2O_3 Decorated TiO_2 Nanotube Confined Pt Nanoparticles with Enhanced Activity for Catalytic Combustion of Ethylene. *J. Mater. Sci.* **2018**, *54*, 4637−4646.
(29) Peng, Q.; Peng, G.; Wu, L.; Li, J.; Wang, X.; Liu, M.; Li, X. Fe_2O_3 Modification Promotes the Photocatalytic Performance of TiO_2 Nanotube Confined Pd Nanoparticles. *J. Photochem. Photobiol., A* **2019**, *380*, 111865.
(30) Chen, M.; Yin, H.; Li, X.; Qiu, Y.; Cao, G.; Wang, J.; Yang, X.; Wang, P. Facet- and Defect-Engineered Pt/Fe_2O_3 Nanocomposite Catalyst for Catalytic Oxidation of Airborne Formaldehyde under Ambient Conditions. *J. Hazard. Mater.* **2020**, *395*, 122628.
(31) Özcan, A.; Atılır Özcan, A.; Demirci, Y.; Şener, E. Preparation of Fe2O3 modified kaolin and application in heterogeneous electro-catalytic oxidation of enoxacin. *Appl. Catal., B* **2017**, *200*, 361−371.
(32) Wang, X.; Feng, J.; Zhang, Z.; Zeng, W.; Gao, M.; Lv, Y.; Wei, T.; Ren, Y.; Fan, Z. Pt Enhanced the Photo-Fenton Activity of $ZnFe_2O_4$/Alpha-Fe_2O_3 Heterostructure Synthesized via One-Step Hydrothermal Method. *J. Colloid Interface Sci.* **2020**, *561*, 793−800.
(33) Zhang, Y.; Chen, J.; Li, X. Preparation and Photocatalytic Performance of Anatase/Rutile Mixed-Phase TiO_2 Nanotubes. *Catal. Lett.* **2010**, *139*, 129−133.
(34) Yamashita, T.; Hayes, P. Analysis of XPS Spectra of Fe^{2+} and Fe^{3+} Ions in Oxide Materials. *Appl. Surf. Sci.* **2008**, *254*, 2441−2449.
(35) Sun, B.; Zhou, W.; Li, H.; Ren, L.; Qiao, P.; Xiao, F.; Wang, L.; Jiang, B.; Fu, H. Magnetic Fe_2O_3/Mesoporous Black TiO_2 Hollow Sphere Heterojunctions with Wide-Spectrum Response and Magnetic Separation. *Appl. Catal., B* **2018**, *221*, 235−242.

https://doi.org/10.1021/acsomega.1c00665
ACS Omega 2021, 6, 11529−11536